Supporting Information

Biomass derived robust Fe$_4$N active sites supported on porous carbons as oxygen reduction reaction catalysts in durable Zn-air batteries

Xiangyu Lu[a], Peixia Yang*[a], Hao Xu[a], Lihui Xiao[a], Lilai Liu[b], Ruopeng Li[a], Elena Alekseeva [c], Jinqiu Zhang[a], Oleg Levin [c], Maozhong An[a].

[a]MIIT Key Laboratory of Critical Materials Technology for New Energy Conversion and Storage, School of Chemistry and Chemical Engineering, Harbin Institute of Technology, Harbin, 150001 China.

[b]College of Environmental and Chemical Engineering, Heilongjiang University of Science and Technology, Harbin, 150022, China.

[c]Institute of Chemistry, St. Petersburg State University, 7/9 Universitetskaya Nab., St. Petersburg, 199034, Russian Federation.

* Corresponding authors: Peixia Yang (yangpeixia@hit.edu.cn)

Experimental Section

Materials

All chemicals used in this study were purchased without further purification.

Characterization

Scanning electron microscopy (SEM, Quanta 200FEG) and transmission electron microscopy (TEM, FEI Talos F200X) were carried out to characterize microstructure. The X-ray diffraction (XRD, Rigaku SmartLab SE Powder Diffractometer) pattern was performed to characterize crystal structure. The Raman spectrum were collected by HR800, JY Company. The nitrogen adsorption/desorption isotherm were conducted on Micromeritics ASAP 2460. X-ray photoelectron spectroscopy (XPS) measurements were characterized by Thermo Kalpha. X-ray absorption spectra (XAS) at Fe K-edge was acquired in fluorescence mode at the BL14W1 at Shanghai Synchrotron Radiation Facility (SSRF).

Electrochemical Measurements

A rotating disk electrode (RDE) and a rotating ring-disk glass carbon electrode (RRDE) were used as the working electrode. A Hg/HgO (alkaline medium) or Hg/Hg_2SO_4 (acidic medium) electrode and a graphite sheet electrode were used as reference and counter electrodes, respectively.

ORR activity was measured by cyclic voltammetry (CV) at a scan rate of 50 mV·s^{-1} and linear sweep voltammetry (LSV) with 1600 rpm at a scan rate of 10 mV·s^{-1} in 0.1 M KOH saturated with O_2/N_2. The accelerated durability test (ADT) was investigated by continuous potential cycling from 0.6 to 1.0 V at a scan rate of 50 mV·s^{-1} in 0.1 M KOH (or 0.1 M $HClO_4$) saturated-O_2 solution.

The electron transfer number (n) and kinetic current density (j_k) were calculated from the Koutecky-Levich (K-L) equation:

$$\frac{1}{j} = \frac{1}{j_L} + \frac{1}{j_K} = \frac{1}{B\omega^{\frac{1}{2}}} + \frac{1}{j_K}$$

$$B = 0.2nFC_O D_O^{\frac{2}{3}} v^{-\frac{1}{6}}$$

Where j, j_K and j_L are measured current density, kinetic-limiting current and diffusion-limiting current density respectively; ω is the rotational speed (rpm) of RDE; F is the Faraday constant (96485 C mol^{-1}); C_O is the O$_2$ concentration (0.1M KOH is 1.2×10^{-3} mol L^{-1}); D_O is the diffusion coefficient of O$_2$ (0.1 M KOH is 1.9×10^{-5} cm^2 s^{-1}); v is the dynamic viscosity of 0.1 M KOH (0.01 cm^2 s^{-1}).

The rotating ring disk electrode (RRDE) was used to measure the hydrogen peroxide yield (H$_2$O$_2$%) and the number of electron transfers (n) according to the following equation:

$$H_2O_2(100\%) = 200\frac{I_R/N}{I_D + I_R/N}$$

$$n = 4\frac{I_D}{I_D + I_R/N}$$

where I_D is the disk current density, I_R is the ring current density, and N is the collection efficiency of the Pt ring (37%).

The OER LSV performance was tested in 0.1 M KOH at a scan rate of 10 mV s^{-1}. Before testing the LSV of OER, the electrodes need to be activated by CV tests with a scan rate of 50 mV s^{-1} in the potential range from 1.1 to 1.5 V (vs RHE). The OER stability of catalysts was measured by by accelerated durability test (ADT). The potential cycles were conducted for 5000 cycles between 1.3 V and 1.7 V in 0.1 M KOH solution.

Density functional theory (DFT) calculations

DFT calculations were performed on Materials studio. The convergence standard for the energy force and maximum displacement was set as 10^{-5} Ha, 0.005Å, respectively. The smearing was set to 0.005 Ha to ensure accurate electronic convergence. For comparison, the DFT calculations of Fe_4N (1 1 1) supported N-doped carbon and Fe (1 1 0) supported N-doped carbon were investigated.

The adsorption energy (E_{ads}) of ORR intermediates is calculated as follows:

$$E_{ads} = E_{total} - E_m - E_{sub}$$

Where the E_{total} is total adsorption energy of the catalyst and species, E_{sub} is the catalyst energy without adsorption, and E_m is the energy of the species.

The pathways on Fe_4N supported N-C systems were calculated in detail according to electrochemical framework developed by Nørskov. The free energy change of every elementary reaction is calculated as follows:

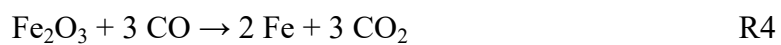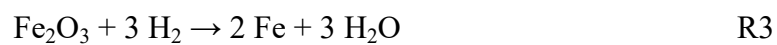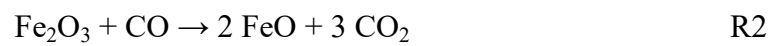$$\Delta G = \Delta E - T\Delta S + \Delta ZPE + \Delta G_{field} + \Delta G_U + \Delta G_{pH}$$

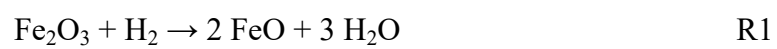Where the ΔE, T, ΔS and ΔZPE are reaction energy, the temperature (289.15 K), the entropy and zero point energy, respectively. The parameters of ΔZPE and ΔS can be calculated according to the vibration frequency of oxygen-contained intermediates. The influence of electric potential on the Gibbs free energy is expressed by $\Delta G_U = -neU$, where n is the number of electrons transferred and U is the electrode potential. In this work, ΔG_{pH} and ΔG_{field} are not involved because they have less contribution to the trends of free energy change.
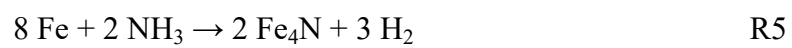
Preparation and tests of Zn-air batteries

The Liquid Zn-air battery was assembled with a uniform nickel foam coated with catalyst ink as an air cathode, 6 M KOH and 0.2 M $(CH_3COO)_2Zn$ as the electrolyte, and a polished Zn plate as an anode. 1.5 mg of catalyst, 1 mg of acetylene black, and 4 mg of activated carbon was added to the mixed solution containing 8 μL of Nafion and 200 μL of isopropanol. Subsequently, the uniform catalyst ink was applied dropwise to the surface of nickel foam as an air cathode. The mass loading of prepared catalysts and commercial 20 wt% Pt/C catalyst is 1.5 mg cm^{-2}. The polarization curves of the batteries were collected using the CHI760E electrochemical workstation in an air environment. The performance of batteries was tested by the LAND CT2001A test system. The discharge-charge cycling stability of the battery at 5 mA cm^{-2} with 10 min per cycle.

The all-solid-state Zn-air battery was assembled with a polished Zn foil as the anode, a catalyst-coated Ni foam as the cathode, and the solid-state electrolyte (gel polymer). 5 g of polyvinyl alcohol (PVA) was added into 45 mL of H_2O under vigorous stirring. Then 5 mL of KOH solution (1 g mL^{-1}) was added into the above solution and was stirried for 40 min at 95 ℃. After freezing for 24 h, the gel was placed at room temperature for 1 h. The performance of all-solid-state batteries was tested by the LAND CT2001A test system.

Supporting Reactions R1–R4:

$$Fe_2O_3 + H_2 \rightarrow 2\ FeO + 3\ H_2O \hspace{4cm} R1$$

$$Fe_2O_3 + CO \rightarrow 2\ FeO + 3\ CO_2 \hspace{4cm} R2$$

$$Fe_2O_3 + 3\ H_2 \rightarrow 2\ Fe + 3\ H_2O \hspace{4cm} R3$$

$$Fe_2O_3 + 3\ CO \rightarrow 2\ Fe + 3\ CO_2 \hspace{4cm} R4$$

Supporting Reactions R5-R6:

$$8\ Fe + 2\ NH_3 \rightarrow 2\ Fe_4N + 3\ H_2 \hspace{4cm} R5$$
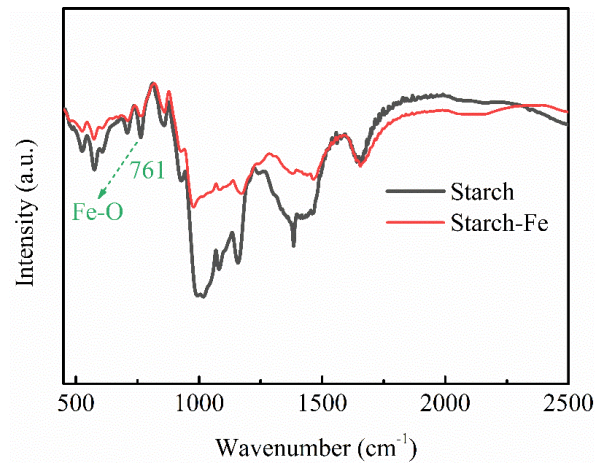
$$2\ ZnO + C \rightarrow 2\ Zn + CO_2 \hspace{4cm} R6$$

Figure S1. FT-IR spectra of the complexes of starch and Fe.

Figure S2. The weighing photograph of the obtained Fe$_4$N@N-C catalyst when the quality of
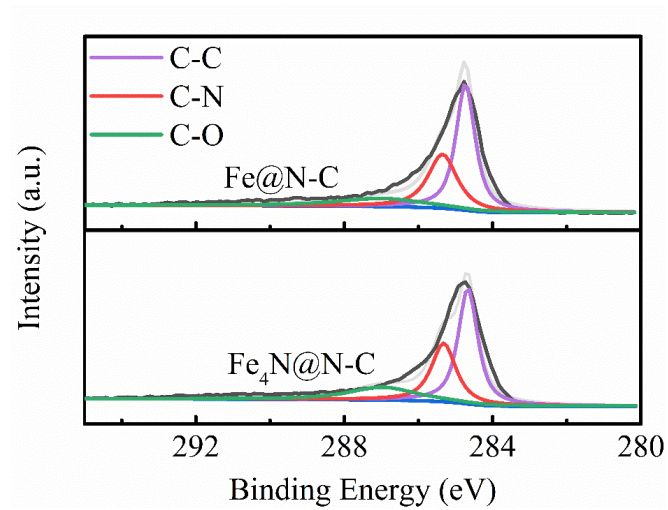
precursors is 6 g.
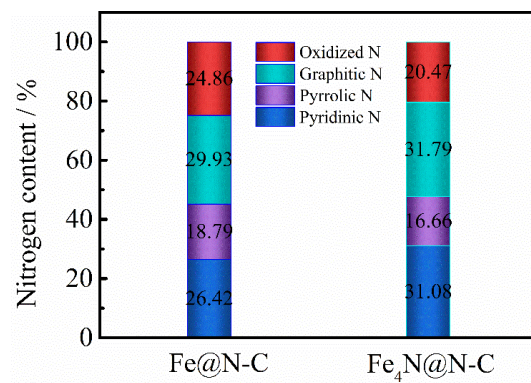
Fig. S3. C 1s XPS spectrum of Fe@N-C and Fe$_4$N@N-C

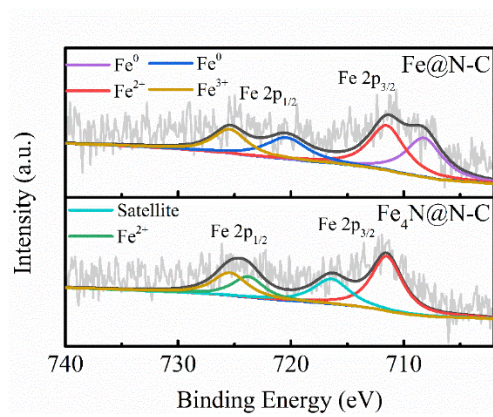**Fig. S4**. Summary of N species contents of Fe@N-C and Fe$_4$N@N-C.

Fig. S5. Fe 2p XPS spectrum of Fe@N-C and Fe$_4$N@N-C.
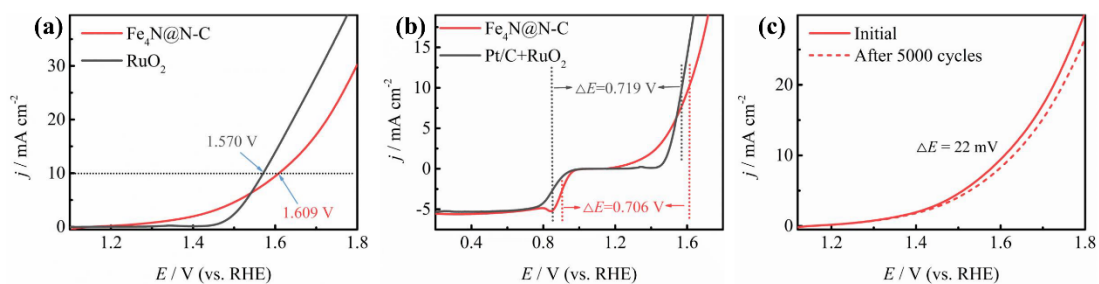
Fig. S6. (a) OER polarization curves of Fe$_4$N@N-C and RuO$_2$ in O$_2$-saturated 0.1 M KOH at 1600 rpm. (b) The entire ORR and OER LSV curves of Fe$_4$N@N-C and RuO$_2$ at 1600 rpm. (c) OER polarization curves of Fe$_4$N@N-C at 1600 rpm with a scan rate of 10 mV s^{-1} before and after 5000 CV cycles (the potential cycles were conducted between 1.3 V and 1.7 V).

Fig. S7. The optimized structure of (a) Fe@N-C and (b)Fe$_4$N@N-C.

Fig. S8. XRD pattern of Fe$_4$N@N-C after 3 M HNO$_3$ etching.

Fig. S9. TEM image of Fe$_4$N@N-C after 3 M HNO$_3$ etching.

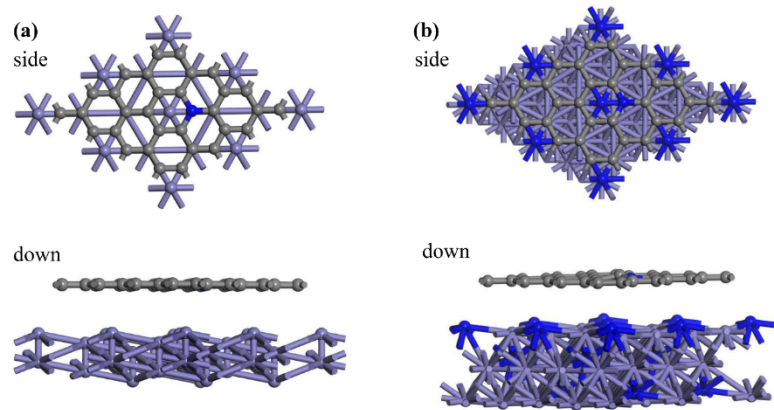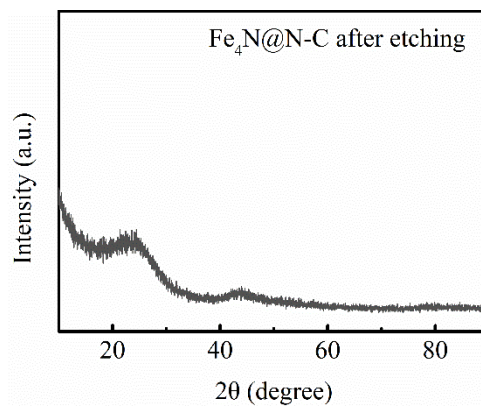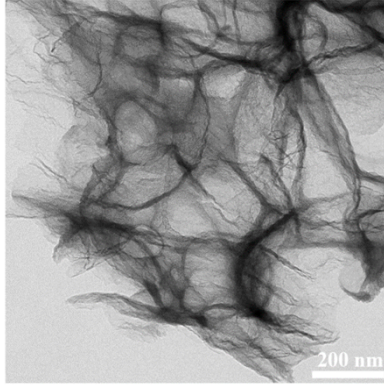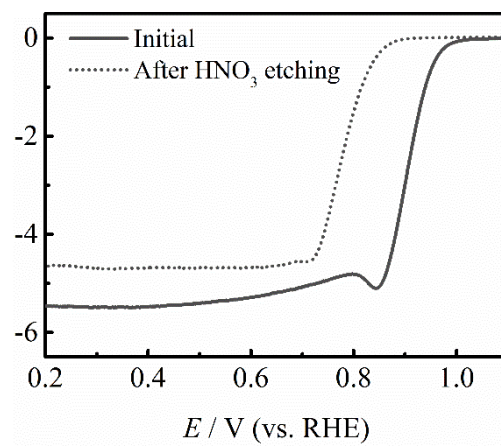**Fig. S10**. Polarization curves of ORR in 0.1 M KOH of $Fe_4N@N-C$ after 3 M HNO_3 etching.

Table S1. Specific surface area and pore parameters of as-prepared materials.

Catalysts	Specific surface area ($m^2\ g^{-1}$)	Micropore area ($m^2\ g^{-1}$)	Pore volume ($cm^3\ g^{-1}$)	Average pore diameter (nm)
Fe@N-C	286.80	225.22	0.2443	3.7671
Fe$_4$N@N-C	377.63	286.90	0.4088	4.6861

Table S2. The content of C, N, O and Fe of the prepared catalysts obtained from XPS

Catalysts (at%)	C	N	O	Fe
Fe@N-C	86.26	6.37	6.36	0.41
Fe$_4$N@N-C	89.56	5.13	4.81	0.51

Table S3. A comparison table of the ORR performance between this work and recently reported Pt-free catalysts in alkaline and acidic medium (vs. RHE)

Materials	$E_{1/2}$ (V) in 0.1 M KOH	$E_{1/2}$ (V) in 0.1 M HClO$_4$ or 0.5 M H$_2$SO$_4$	References
Fe$_4$N@N-C	0.903	0.761 (HClO$_4$)	This work
Cu-NSDC SACs	0.84	/	[1]
Fe$_2$-N/CNTs-850	0.846	/	[2]
Sb$_1$/NG(O)	0.86	/	[3]
Fe0.5Co@HOMNCP	0.903	0.76 (H$_2$SO$_4$)	[4]
ZnCu-N-C (1000)	0.87	/	[5]
NHC-900	0.835	/	[6]
Co@NrC-0.3	0.85	/	[7]
NSC/Co$_9$S$_8$-200	0.83	/	[8]
4.2-FeSA	0.901	/	[9]
p-Fe–N-CNF	/	0.74 (HClO$_4$)	
CuSA/CuCT@NPC	0.88	0.70 (HClO$_4$)	[10]
Fe/Ni(1:3)-NG	0.842	/	[11]
NC-Co SA	0.87		[12]

CoN4/NG	0.87	/	13
CoNi-SAs/NC	0.76	/	14
Fe/N-G#4	0.852	/	15
Fe–Nx ISAs/GHSs	0.89	/	16
TimB-Fe5-C	0.89	0.78 ($HClO_4$)	17
Fe SA/NPCs	0.83	0.78 (H_2SO_4)	18
NFC@Fe/Fe3C-9	0.87	0.73 ($HClO_4$)	19
NSPC-0.2–900	0.84	0.71 ($HClO_4$)	20
porous CS	0.74	0.092 V more negative than that of Pt/C	21

Table S4. A comparison table of the ORR durability between this work and recently reported Pt-free catalysts in alkaline and acidic medium.

Materials	$\triangle E_{1/2}$ in 0.1 M KOH	$\triangle E_{1/2}$ in 0.1 M $HClO_4$	References
Fe$_4$N@N-C	1 mV (5000 cycles)	7 mV (5000 cycles)	This work
Fe$_2$-N/CNTs-850	26 mV (3000 cycles)	/	2
4.2-FeSA	6 mV (5000 cycles)	/	9
CuSA/CuCT@NPC	6 mV (5000 cycles)	/	10
Fe/Ni(1:3)-NG	23 mV (3000 cycles)	/	11
3D Fe/N-G#4	13 mV (3000 cycles)	/	15
Fe–Nx ISAs/GHSs	14 mV (5000 cycles)		16
NFC@Fe/Fe3C-9	16 mV (30000 cycles)	27 mV (30000 cycles)	19
porous CS	10 mV (1000 cycles)	/	21

Table S5. Summary of the performance of aqueous and solid state ZABs based on Pt-free athode catalysts.

Materials	OCV of Aqueous ZABs (V)	Aqueous ZABs Peak power density (mW cm^2)	Solid state ZABs Peak power density (mW cm^2)	References
Fe$_4$N@N-C	**1.493**	**182**	**121**	**This work**
Fe$_{0.5}$Co@HOMNCP	1.619	134	/	[4]
ZnCu-N-C (1000)	1.51	156.2	/	[5]
Co/MnO@NC	1.5	146	/	[22]
NHC-900	1.345	107	/	[6]
Co@NrC-0.3	1.47	168	/	[7]
NSC/Co$_9$S$_8$-200	1.47	176	/	[8]
CoSAs/N-CNS	/	157.7	/	[23]
4.2-FeSA	/	211.4	132	[9]
Fe/Ni(1:3)-NG	1.50	164.1		[11]
NC-Co SA	1.41	/	20.9	[12]
CoN$_4$/NG	1.51	115	28	[13]
CoNi-SAs/NC	1.45	101.4	/	[14]
3D Fe/N-G#4	1.522	168.4	/	[15]
Fe-N-C-700	1.424	/	70	[24]
CoNx/Zn-NC	1.3	164.1	/	[25]

Table S6. Summary of the durability of aqueous ZABs based on Pt-free athode catalysts.

Materials	Charge and discharge operating time	References

Fe$_4$N@N-C	1032h / 6198 cycles (5 mA cm^{-2})	This work
Fe-N-HPC	120 h (2 mA cm^{-2})	[4]
NHC-900	12 h (10 mA cm^{-2})	[6]
Co@NrC-0.3	40 h (2 mA cm^{-2})	[7]
NSC/Co$_9$S$_8$-200	120 h / 386 cycles (10 mA cm^{-2})	[8]
CoSAs/N-CNS	150 h / 900 cycles (5 mA cm^{-2})	[23]
4.2-FeSA	450 h / 2000 cycles (10 mA cm^{-2})	[9]
Fe/Ni(1:3)-NG	120 h (5 mA cm^{-2})	[11]
Co/MnO@NC	400 h / 600 cycles (20 mA cm^{-2})	[22]
NC-Co SA	180 h / 570 cycles (10 mA cm^{-2})	[12]
CoN$_4$/NG	100 h (10 mA cm^{-2})	[13]
CoNi-SAs/NC	96 cycles (5 mA cm^{-2})	[14]
3D Fe/N-G#4	60 h / 183 cycles (20 mA cm^{-2})	[15]
CoNx/Zn-NC	115 h (10 mA cm^{-2})	[25]

Reference

1.   H. Zhang, Q. Sun, Q. He, Y. Zhang, X. He, T. Gan and H. Ji, *Nano Research*,

2022, DOI: 10.1007/s12274-022-4289-3.

2. C. Li, Y. Wu, M. Fu, X. Zhao, S. Zhai, Y. Yan, L. Zhang and X. Zhang, *ACS Applied Energy Materials*, 2022, **5**, 4340-4350.

3. Y. Gu, B. Xi, H. Zhang, Y. Ma and S. Xiong, *Angew Chem Int Ed Engl*, 2022, DOI: 10.1002/anie.202202200.

4. W. Li, B. Liu, D. Liu, P. Guo, J. Liu, R. Wang, Y. Guo, X. Tu, H. Pan, D. Sun, F. Fang and R. Wu, *Adv Mater*, 2022, **34**, e2109605.

5. M. Qian, M. Guo, Y. Qu, M. Xu, D. Liu, C. Hou, T. T. Isimjan and X. Yang, *Journal of Alloys and Compounds*, 2022, **907**.

6. L. Wang, S. Q. Guo, Z. Hu, B. Shen and W. Zhou, *ChemCatChem*, 2022, DOI: 10.1002/cctc.202200063.

7. J. Yu, Y. Dai, Z. Zhang, T. Liu, S. Zhao, C. Cheng, P. Tan, Z. Shao and M. Ni, *Carbon Energy*, 2022, DOI: 10.1002/cey2.171.

8. Q. Zheng, Y. Xiong, K. Tang, M. Wu, H. Hu, T. Zhou, Y. Wu, Z. Cao, J. Sun, X. Yu and C. Wu, *Nano Energy*, 2022, **92**.

9. X. Wu, Q. Wang, S. Yang, J. Zhang, Y. Cheng, H. Tang, L. Ma, X. Min, C. Tang, S. P. Jiang, F. Wu, Y. Lei, S. Ciampic, S. Wang and L. Dai, *Energy & Environmental Science*, 2022, **15**, 1183-1191.

10. Z. Yang, K. Jiang, G. Tong, C. Ke, H. Wu, P. Liu, J. Zhang, H. Ji, J. Zhu, C. Lu and X. Zhuang, *Chemical Engineering Journal*, 2022, **437**.

11. Y. Ma, H. Fan, C. Wu, M. Zhang, J. Yu, L. Song, K. Li and J. He, *Carbon*, 2021, **185**, 526-535.

12. W. Zang, A. Sumboja, Y. Ma, H. Zhang, Y. Wu, S. Wu, H. Wu, Z. Liu, C. Guan, J. Wang and S. J. Pennycook, *ACS Catalysis*, 2018, **8**, 8961-8969.

13. L. Yang, L. Shi, D. Wang, Y. Lv and D. Cao, *Nano Energy*, 2018, **50**, 691-698.

14. X. Han, X. Ling, D. Yu, D. Xie, L. Li, S. Peng, C. Zhong, N. Zhao, Y. Deng and W. Hu, *Adv Mater*, 2019, **31**, e1905622.

15. C. Wang, Z. Li, L. Wang, X. Niu and S. Wang, *ACS Sustainable Chemistry & Engineering*, 2019, **7**, 13873-13885.

16. X. Qiu, X. Yan, H. Pang, J. Wang, D. Sun, S. Wei, L. Xu and Y. Tang, *Adv Sci (Weinh)*, 2019, **6**, 1801103.

17. X. Lin, P. Peng, J. Guo, L. Xie, Y. Liu and Z. Xiang, *Nano Energy*, 2021, **80**.

18. H. Yang, Z. Li, S. Kou, G. Lu and Z. Liu, *Applied Catalysis B: Environmental*, 2020, **278**, 119270.

19. M. Karuppannan, J. E. Park, H. E. Bae, Y. H. Cho and O. J. Kwon, *Nanoscale*, 2020, **12**, 2542-2554.

20. L. Wang, K. Liang, L. Deng and Y.-N. Liu, *Applied Catalysis B: Environmental*, 2019, **246**, 89-99.

21. C. Su, Y. Liu, Z. Luo, J.-P. Veder, Y. Zhong, S. P. Jiang and Z. Shao, *Chemical Engineering Journal*, 2021, **406**.

22. Y. Niu, X. Teng, S. Gong, X. Liu, M. Xu and Z. Chen, *Energy Storage Materials*, 2021, **43**, 42-52.

23. D. Wang, M. Yuan, J. Xu, Y. Li, K. Shi, H. Yang, H. Li and G. Sun, *ACS Sustainable Chemistry & Engineering*, 2021, **9**, 16956-16964.

24. T. Chen, J. Wu, C. Zhu, Z. Liu, W. Zhou, C. Zhu, C. Guan and G. Fang, *Chemical Engineering Journal*, 2021, **405**.
25. L. Xu, D. Deng, Y. Tian, H. Li, J. Qian, J. Wu and H. Li, *Chemical Engineering Journal*, 2021, **408**.